Gain saturation of nickel-like silver and tin x-ray lasers by use of a tabletop pumping laser system

Tetsuya Kawachi,[1] Masataka Kado,[1] Momoko Tanaka,[1] Akira Sasaki,[1] Noboru Hasegawa,[1] Alexander V. Kilpio,[2] Sinichi Namba,[1] Keisuke Nagashima,[1] Peixiang Lu,[1] Kenjiro Takahashi,[1] Huajing Tang,[3] Renzhong Tai,[1] Maki Kishimoto,[1] Masato Koike,[1] Hiroyuki Daido,[1] and Yoshiaki Kato[1]

[1]*Advanced Photon Research Center, Kansai Research Establishment, Japan Atomic Energy Research Institute, 8-1, Umemidai, Kizu, Kyoto, 616-0215, Japan*

[2]*General Physics Institute, Russian Academy of Science, 38 Vavilov Street, 117942, Moscow, Russia*

[3]*Institute of Laser Engineering, Osaka University, Suita, Osaka, 565-0871, Japan*

(Received 24 January 2002; published 24 September 2002)

Silver and tin slab targets were irradiated by line-focused chirped pulse amplification glass laser light. In this experiment, the laser pulses consisted of two pulses with 4 ps duration, separated by 1.2 ns. Strong amplification in the nickel-like silver and tin x-ray lasers at the wavelengths of 13.9 and 12.0 nm was demonstrated with pumping energy of 12 and 14 J, respectively, and gain-saturation behavior could be seen. A hydrodynamics simulation coupled with a collisional-radiative model was performed under the present experimental conditions, and the calculated result was compared with the experimental results.

DOI: 10.1103/PhysRevA.66.033815 PACS number(s): 42.55.Vc, 42.60.By, 52.50.Jm

I. INTRODUCTION

Since the demonstration of soft x-ray amplification [1,2], x-ray laser research has been intensively pursued experimentally and theoretically. The development of highly efficient and intense output in the short-wavelength region using a compact pumping system is one of the most important objectives. Recently, using small-size CPA Nd:glass lasers with an energy of around 15 J, strong amplifications of x rays have been reported in transient collisional excitation (TCE) lasers for the wavelength region up to 13.9 nm [3–8]. In neonlike ion lasers, Kalachnikov *et al.* observed gain saturation in a neonlike titanium laser at a wavelength of 32.6 nm [3]. In the nickel-like ion lasers, gain saturation has been reported by Dunn *et al.* for several *z* elements, e.g., molybdenum, palladium, and silver [4–6], and by Klisnick *et al.* for a silver laser [7,8]. In the shorter-wavelength region, to the author's knowledge, MacPhee *et al.* demonstrated gain saturation of a nickel-like tin laser at a wavelength of 12.0 nm with a pumping energy greater than 60 J [9]. However, this pumping energy may be beyond the performance of a tabletop laser system at the present time. Demonstration of gain saturation in this wavelength region using a small pumping system is valuable for the development of highly efficient compact x-ray lasers, and comparison of the experiments with a detailed theoretical model is important to realize the pumping mechanism of TCE lasers and to optimize the lasing condition.

Another important point for development of highly efficient compact x-ray lasers is the employment of traveling-wave pumping, by which substantial improvement in output energy of the x-ray beam is expected. In addition, since the observed gain coefficients and the output x-ray beam intensity under conditions without traveling-wave pumping may be affected by the gain duration of the lasing medium, comparison of the experimental result with theoretical models may become indirect. This difficulty can be removed by adopting traveling-wave pumping.

From a technical point of view, traveling-wave pumping has been generated by tilting a grating of the grating pair in the pulse compressor [10] or by an additional grating with a small number of grooves (~50 lines/mm) after the final amplifier [11]. However, tilting a grating or installation of an additional grating may induce diffraction of the laser beam, and the spectral bandwidth in the left- or right-hand side of the laser beam is reduced. This leads to elongation of the pulse duration in these portions and inhomogeneous intensity along the line focus, which is unfavorable for x-ray laser experiments. Furthermore, the low diffraction efficiency of the additional grating with a small number of grooves (typically ~50%) requires much larger pumping energy, which goes against development of compact x-ray laser systems. In order to avoid it, a step mirror can be used to generate a quasitraveling wave. In a transient collisional excitation scheme, e.g., in the nickel-like palladium laser at a wavelength of 14.7 nm, the gain duration has been estimated to be ~7 ps [12], and from the scaling law of the temporal behavior of ions in ionizing plasmas, i.e., $t \propto z_{\mathrm{eff}}^{-4}$, the gain duration becomes shorter for higher-*z* elements [13]. Since the time step of the quasitraveling wave has to be shorter than or comparable with the gain duration, we have to take the expected gain duration into account when we design the time step of the quasitraveling wave.

Recently, we demonstrated substantial amplification at a wavelength of 12.0 nm with a pumping energy of ~14 J [14]. In this experiment, the target is irradiated by double pulses with a few picoseconds duration, separated by 1.2 ns, whereas almost all the other experiments employ a prepulse with long (~500 ps) duration and a main pulse with a few picoseconds duration. In order to compare our experimental result with a theoretical code and to realize the pumping mechanism, we conduct an experiment using quasitraveling-wave pumping. We have nickel-like silver (13.9 nm) and tin (12.0 nm) x-ray lasers as our objectives, using a step mirror with 4 ps step to generate a quasitraveling wave. The measured gains in the x-ray laser lines are compared with the result without traveling-wave pumping, and the experimental output intensity of the x-ray beam is compared with the theoretical intensity. By use of our hydrodynamics code coupled with a collisional-radiative (CR) model, we discuss the mechanism of generation of the gain under the present experimental conditions.

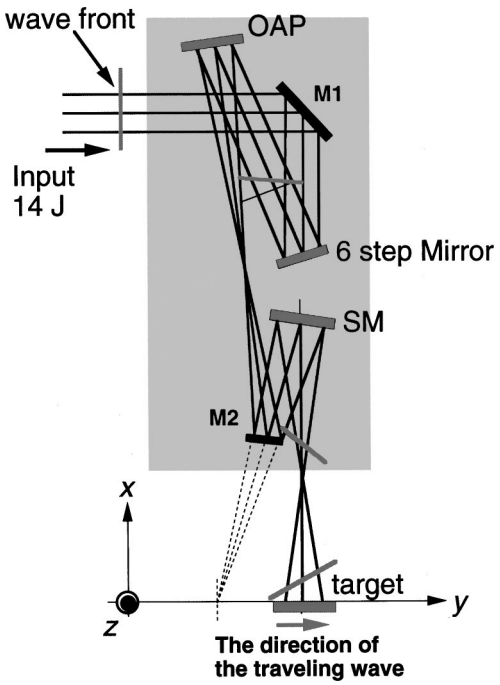

FIG. 1. A schematic of our line-focusing system. $M1$ and $M2$ are steering planar mirrors, and OAP and SM represent an off-axis parabolic mirror and a spherical mirror, respectively. The six-step mirror is installed just before the OAP.

II. EXPERIMENT AND RESULT

Our chirped pulse amplification (CPA) Nd:glass laser system consists of a mode-locked Ti:sapphire oscillator (Spectra Physics, Tsunami), a four-pass pulse expander, a Ti:sapphire regenerated amplifier (Positive Light, TSA-10), two amplifier chains of phosphate glass rods, and two pulse compressors. The central wavelength is 1053 nm and the spectral bandwidth after the amplifier chain is 3.5 nm. Each beamline provides a prepulse and a main pulse with variable pulse separation. The maximum output energy is 20 J for each beamline after the compressors, and the pulse duration is variable from 1 to 30 ps. The details of the pumping laser system are given in Ref. [15].

In the present experiment, one beam of the Nd:glass CPA laser was used to irradiate a silver or a tin slab target. A schematic figure of our line-focusing system is shown in Fig. 1. The line-focusing system was based on an off-axis parabolic mirror (focal length of 772 mm) and an off-axis spherical mirror (curvature of 1000 mm), which made a line focus with 5.6 mm length and 20 μm width at the target position [16]. We installed a six-step mirror (Optical Surface Inc.) just before the off-axis parabolic mirror to generate a quasitraveling wave. This step mirror consisted of six blocks and each was connected to a base plate by optical contact. The blocks were parallel to each other with an accuracy of 0.05 mrad in the vertical direction and of 0.1 mrad in the horizontal direction. The size of the blocks was 25 mm width, 150 mm height, and the difference of thickness between the neighboring blocks was 600 μm. The angle of incidence was 11° with respect to the surface normal, which led to an optical delay of 4.07 ps between the laser beams reflected from neighboring blocks. The reflection from each block corresponded to a length of 1.2 mm in the line focus. The velocity of the traveling wave at the target position was measured to be $0.98c \pm 0.08c$ by use of a visible streak camera with a time resolution of 2 ps (Hamamatsu-Photonics Model C4302), where c is the speed of the light. Since our streak camera was insensitive to the fundamental laser light (1.053 μm), a potassium dihydrate phosphate crystal was put just before the target position, and the second harmonic was used. The speed of amplified x rays in high-density plasmas might be different from that in vacuum; however, for the 13.9 and 12.0 nm lines, under a plasma density of 10^{21} cm^{-3}, the difference from the speed in vacuum is negligibly small. The quality of the width of the line focus was measured using a 1-mm-thick titanium target, which was irradiated by a single pulse with 4 ps duration and 10 J energy. From the trace of the laser irradiation on the titanium target, the width of the line focus was around 20 μm, and we are assured that no interference pattern can be seen.

A silver or tin slab target was put at the focus position with an accuracy of 20 μm in the x direction and an accuracy of 2 mrad along the z axis, where x and z directions are referred to Fig. 1. The laser pulses consisted of two pulses, and the duration of each pulse was 4 ps with a pulse-to-pulse separation of 1.2 ns. The total pumping energy was set to 12 J for the silver laser and 14 J for the tin laser. The energy ratio of the prepulse to that of the main pulse was 1:7. Our previous experiment showed that this pulse pattern was favorable for generating an amplified x ray [14]. The irradiance of the prepulse and the main pulse on target were 3.0×10^{14} and 2.3×10^{15} W/cm^2, respectively, for the silver laser and 3.6×10^{14} and 2.7×10^{15} W/cm^2, respectively, for the tin laser. The contrast ratio of the ASE level to the peak intensity was measured to be $(3-5) \times 10^{-4}$, i.e., the pedestal level of the main pulse was around $(6 \times 10^{11}) - 10^{12}$ W/cm^2, which affected the plasma condition. The role of the pedestal level will be discussed later. Shot-to-shot fluctuation in the pumping energy was less than 7% for the silver case and less than 10% for the tine case. The output x-ray laser line, which correspond to the transition $4p$-$4d$, was observed by use of a grazing-incidence spectrometer in the y direction. The spectrometer consisted of a spherical mirror with a curvature of 3520 mm, an entrance slit of 50 μm width, and an uneven-spacing holographic laminar grating (average number of grooves is 1200 lines/mm), fabricated with Shimadzu [17] as a collaborator. The absolute diffraction efficiency of the grating was calibrated using the synchrotron radiation source of Ritsumeikan University (AURORA). The detector was a back-illuminated x-ray charge-coupled device (CCD) (Princeton Instruments, Model SX1024), whose sensitivity is proportional to the incident photon number for photoelectron counts less than 60 000 counts/pixel. The resolution in wavelength was 0.02 nm at a wavelength of 15 nm. The acceptance angle of the spectrometer was ± 10 mrad in the horizontal direction and ± 2.5 mrad in the vertical direction. In the spectrum taken by this spectrometer, the horizontal length of the spectrum on the CCD represented the horizontal beam divergence of the spectral line from the plasma.

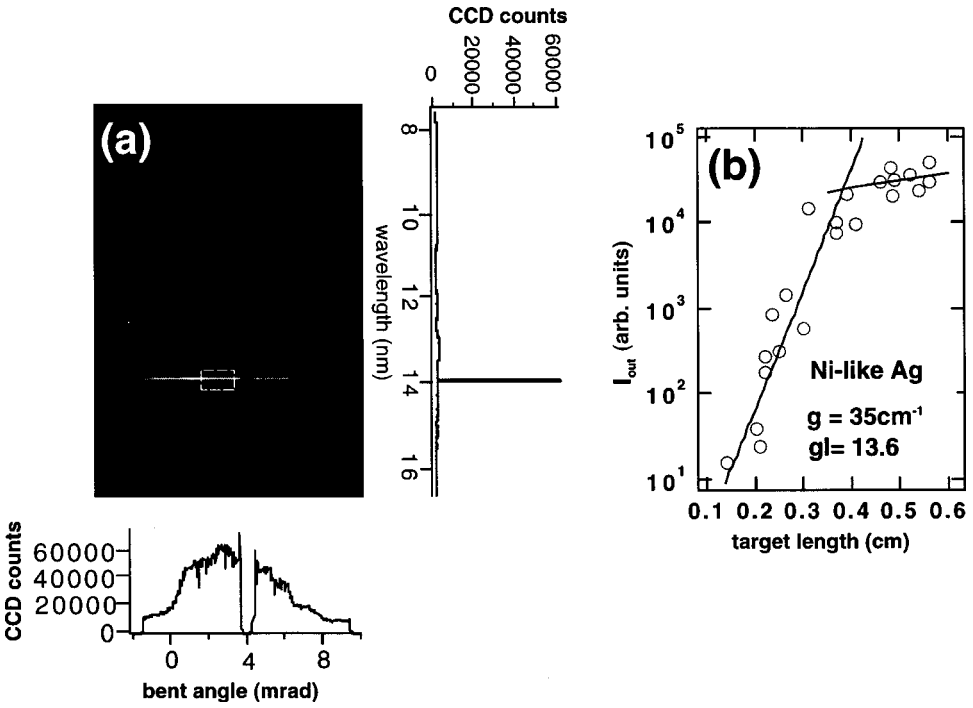

FIG. 2. (a) Typical spectrum of the 13.9 nm line on the CCD. The target length is 5 mm. The horizontal beam profile is also shown. The dip in the horizontal beam profile is a shadow of the frame of the $Y+Si_3N_4$ filter. (b) The output of the 13.9 nm line for various target lengths. The gain coefficient was estimated to be ~ 35 cm^{-1}, and gain-saturation behavior can be seen for targets longer than 3.9 mm.

Figure 2(a) shows a typical spectrum of the nickel-like silver laser at 13.9 nm. In order to avoid saturation of the sensitivity of the CCD, the x-ray laser light was attenuated using a 0.3-μm-thick yttrium filter fabricated on a 0.2-μm-thick Si_3N_4 filter. The transmittance of this filter was measured to be 9% at 13.1 nm using an aluminum plasma generated by a neodymium-doped yttrium aluminum garnet (Nd:YAG) laser with a duration of 8 ns. We averaged over the photoelectron counts of the 30 pixels around the peak [see the dotted area in Fig. 2(a)] in the horizontal direction, and the spectral profile was fitted by a Gaussian curve to derive the relative outputs of the x-ray laser light. We measured the output x-ray laser light for various plasma lengths and plotted them in Fig. 2(b). The gain coefficient g derived from the Linford fitting formula [18] was 35 ± 3 cm^{-1}, and a gain-length product gl of 13.6 ± 1.2 was achieved for the 3.9-mm-length target. g and gl are improved compared with our previous result without traveling-wave pumping: $g=24$ cm^{-1} and $gl\sim 10$ for a 4-mm-length target. In Fig. 2(b), a gain-saturation-like behavior can be seen for target lengths longer than 3.9 mm. In this region, shot-by-shot fluctuation of the output x ray was around $\pm 40\%$, which might be due to the shot-by-shot fluctuation of the pumping energy and the horizontal beam profile of the output x ray.

A similar experiment was performed for the tin laser. In order to avoid saturation of the sensitivity of the CCD for the 12.0 nm line, we used the second-order light of the x-ray laser at 24.0 nm. The detection efficiency for the second-order light was measured to be 1/9.5 of that for the first-order light. A typical spectrum is shown in Fig. 3(a). We measured the output of the second-order x-ray laser light for various target lengths, and plot them in the same way as in the silver case in Fig. 3(b). The gain coefficient derived from fitting by use of Linford formula was 30 ± 1.5 cm^{-1}, and the achieved gain-length product was 13.2. The result is improved compared with our previous results without traveling-wave pumping [14], in which the gain and gain-length product were $g=14$ cm^{-1} and $gl\sim 8$, respectively.

III. DISCUSSION

A. Discussion of the gain-saturation behavior

In Fig. 2(a), gain-saturation-like behavior can be seen for target lengths longer than 3.9 mm. In order to be sure that it is gain saturation, we estimated the output intensity of the x-ray laser light at the edge of the gain medium. The size of the gain region and the output energy were measured using a combination of a spherical and two planar Mo/Si multilayer mirrors and a back-illuminated CCD, and they were 7.0×10^3 μm^2 and around 25 ± 10 μJ, respectively. The details of the measurement will be published elsewhere [19]. In order to estimate the gain duration, we constructed a one-dimensional ray-tracing code including x-ray amplification. We assumed a flat-top temporal gain profile with a peak gain of 35 cm^{-1} and assumed that the length of the plasma was 3.9 mm. The plasma column was divided into cells of 3 μm length, and in each cell amplification of the x ray was calculated. The effects of diffraction of the x ray and gain saturation in the gain medium were not included. We changed the gain duration, and in each case the x-ray outputs were calculated for the cases with pure traveling-wave pumping, I_{TW}, and without it, I_{NTW}. The intensity ratios $I_{\mathrm{NTW}}/I_{\mathrm{TW}}$ are shown in Fig. 4. The ratio given by the experiment is also plotted, resulting in a gain duration of ~ 8 ps, which is consistent with the calculation in Ref. [12]. This together with the experimental results (output energy of the lasing line and the size of the gain region) leads to the experimental output intensity of $(2.7-6.3)\times 10^{10}$ W/cm^2.

The experimental output intensity was compared with the theoretical saturation intensity. Under the assumption that the

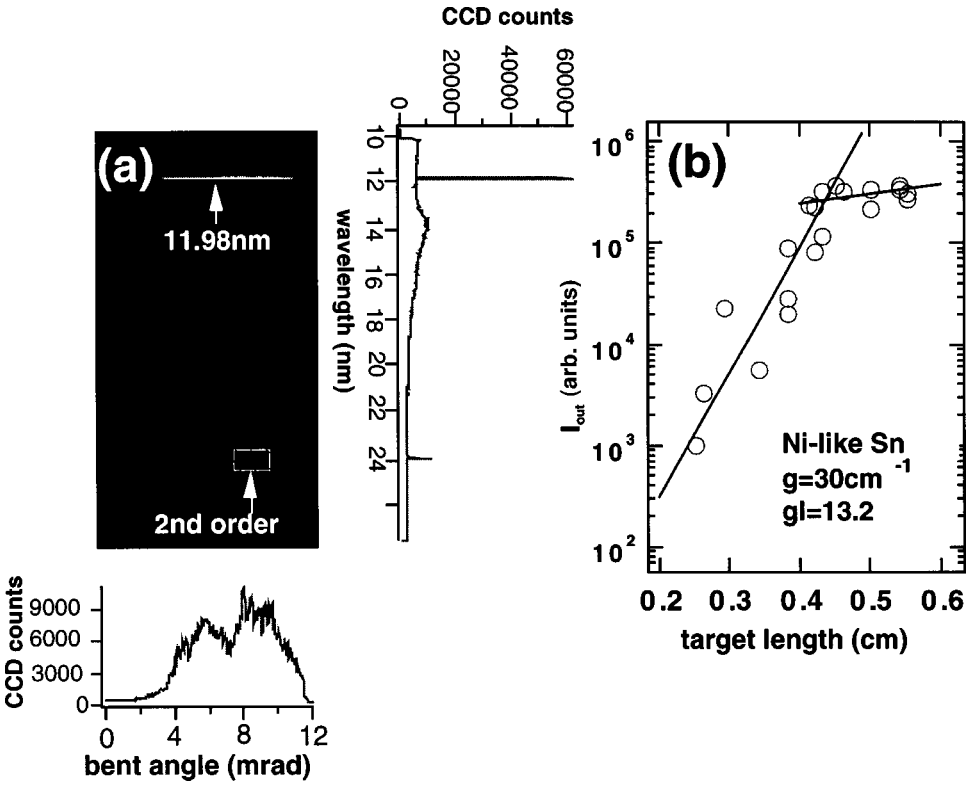

FIG. 3. (a) Typical spectrum of the 12.0 nm line on the CCD. The target length is 4.3 mm. The horizontal beam profile of the second-order light is also shown. (b) The output of the 12.0 nm line for various target lengths. The gain coefficient was estimated to be ~ 30 cm^{-1}, and gain-saturation behavior can be seen for targets longer than 4.4 mm.

spectral line profile is determined by homogeneous (collision and natural) broadening, the saturation intensity I_{sat} at the center frequency of the line profile can be expressed as [20]

$$I_{\mathrm{sat}}=\frac{h\nu}{\sigma_{\mathrm{se}}\tau_2}=\frac{h\nu}{[\lambda^2(\tau_1+\tau_2)/4\pi^2 t_{\mathrm{spont}}]\tau_2}, \tag{1}$$

where $h\nu$ is the photon energy of the x ray, σ_{se} is the stimulated emission cross section, τ_1 and τ_2 are the collisional-radiative destruction times of the lower and upper lasing levels, respectively, λ is the wavelength of the lasing line, and t_{spont} is the decay time of the spontaneous transition of the lasing line. However, in the present case, as mentioned below, the intrinsic spectral profile of the laser line is determined by convolution of the homogeneous and inhomogeneous (Doppler) broadening. Under these conditions it may be better to treat the effect of the spectral profile in the calculation, and the amplification gain averaged over frequency is expressed as follows [21]:

$$g=\Delta N\sigma_{\mathrm{se}}$$
$$=\Delta N^0\frac{\lambda^2}{8\pi t_{\mathrm{spont}}}\int_{-\infty}^{\infty}\int_{-\infty}^{\infty}\frac{p(\nu_\xi)d\nu_\xi}{[1/L(\nu)^\xi]+(\phi\lambda^2 I_\nu/8\pi h\nu)}d\nu, \tag{2}$$

where ΔN and ΔN^0 are the population inversion densities with and without the laser field, respectively, I_ν is the intensity of the amplified x ray, and $\phi=(\tau_2/t_{\mathrm{spont}})[1+(1-\tau_2/t_{\mathrm{spont}})\tau_1/\tau_2]$. It is noted that, since $\tau_2 \ll t_{\mathrm{spont}}$ in the typical gain region, ϕ can be expressed as $(\tau_1+\tau_2)/t_{\mathrm{spont}}$. $P(\nu_\xi)$ is a Gaussian profile corresponding to the ion temperature T_i, and $L(\nu)^\xi$ is a Lorentzian profile of the ensemble of ions in a homogeneous packet ξ,

$$L(\nu)^\xi=\frac{\Delta\nu/2\pi}{(\nu-\nu_\xi)^2+(\Delta\nu/2)^2}. \tag{3}$$

With the typical plasma parameters of the gain region, $T_e=500$ eV, $T_i=150$ eV, and $n_e=5\times10^{20}$ cm^{-3}, which are

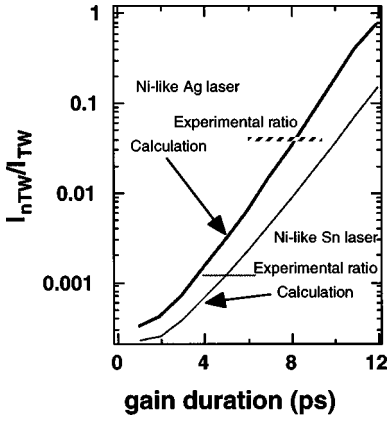

FIG. 4. Calculated ratio of the x-ray laser output without traveling-wave pumping to that with traveling-wave pumping for various gain durations. Experimental ratios are also plotted. The thick and thin solid curves are calculated results for the silver and tin lasers, respectively. The dotted and thin solid lines are experimental ratios for the silver laser at a target length of 3.9 mm and the tin laser at 4.4 mm, respectively. The peak gain is assumed to be 35 cm^{-1} for the silver laser and 30 cm^{-1} for the tin laser. The derived gain duration is about 8 ps for the silver laser and 5 ps for the tin laser.

determined by the HYADES one-dimensional (1D) hydrodynamics code [22], we derive $\tau_2 = 0.153$ ps, $\tau_1 = 0.150$ ps, and $t_{spont} = 4.7$ ps by use of the HULLAC code [23]. This leads to an inhomogeneous width [full width at half maximum (FWHM)] of 13 mÅ and a homogeneous width (FWHM) of 14 mÅ.

The saturation intensity I_{sat} is assumed to be the intensity at which the gain coefficient becomes half its final value. We take the numerical integral of Eq. (2) for given I_ν values, and the saturation intensity of 9.3×10^{10} W/cm^2 is obtained for the typical gain region. The calculated value is higher by a factor of 1.5–3.5 than the present experimental result [$(2.7-6.3)\times10^{10}$ W/cm^2]. This discrepancy may be due to the uncertainty of the electron density of the gain region. Indeed, under the assumption of $n_e = 4\times10^{20}$ cm^{-3}, the calculated saturation intensity is $I_{sat} = 6.2\times10^{10}$ W/cm^2, which is consistent with the experimental value including the error bar. It is noted that another result by Zhang *et al.* [24] shows that the experimental and theoretical saturation intensities are is 6.9×10^{10} and 2.8×10^{10} W/cm^2, respectively, for $n_e = 5.7\times10^{20}$ cm^{-3}. Under the same electron density, our calculated result is 1.1×10^{11} W/cm^2, which is almost consistent with the experimental value, differing by a factor of 1.6. However, the theoretical estimation in Ref. [24] is smaller by a factor of ~4 than our estimation; rather it is consistent with an estimation by use of Eq. (1), which is 3.0×10^{10} W/cm^2 in the present gain region. The conversion efficiency of the output x-ray laser in the present case, which is defined as the ratio of the output energy to the input energy, is 2.0×10^{-6}.

The output intensity of the 12.0 nm line was also estimated. The output energy was derived from a comparison of the CCD counts of the 12.0 nm line with those of the silver laser, where we used the diffraction efficiency of the grating of our spectrometer [17] and the sensitivity of the CCD. The reflectivity of the spherical mirror in the spectrometer is almost constant for 12.0–13.9 nm under the grazing condition (the angle of incidence was 87° with respect to the surface normal). The estimated output energy was 17 ± 7 μJ and the conversion efficiency was 1.2×10^{-6}. The gain duration of 5 ps is derived in the same way as in the silver case (see Fig. 4), and the size of the gain region was assumed to be the same as that of the silver laser, which led to the output intensity of $(2.9-6.8)\times10^{10}$ W/cm^2. This value is almost consistent with the calculated saturation intensity using the plasma parameters of the typical gain region, an electron temperature of 500 eV and electron density of 7×10^{20} cm^{-3}. It should be noted that the present result was obtained by use of a tabletop pumping system and that the present *g* and *gl* are almost equivalent to the result by MacPhee *et al.* obtained with a pumping energy of 60 J [9].

B. Theoretical calculation under the present experimental conditions

In the present experiment, we employed double-pulse irradiation with a pulse duration of a few picoseconds. Since the intensity of the main pulse exceeds 10^{15} W/cm^2, the pedestal level becomes around 10^{12} W/cm^2 under the contrast ratio of $(3-5)\times10^{-4}$, and the plasma condition may be affected by the presence of the pedestal. We include this effect in our calculation and calculate the plasma parameters and the gain coefficient of the x-ray laser under laser irradiation conditions that are similar to the present experimental conditions. We take the nickel-like tin x-ray laser as an example.

The plasma parameters and level populations of the ions are investigated theoretically using the HYADES 1D hydrodynamics code [22] and the WHIAM (web oriented hierarchical atomic model) code [25]. We treat the detailed level structure of the nickel-like ion and the averaged level structure for other charge states in our atomic model. For instance, we have a total number of approximately 300 levels from palladiumlike to argonlike ions, including 150 fine-structure sublevels in the copper-, nickel-, and cobaltlike ions. For the nickel-like ions, the level energies, the probabilities of radiative decay and autoionization, and the rate coefficients of electron impact ionization, excitation-deexcitation, three-body recombination, and radiative recombination are calculated using the HULLAC code [23]. For other charge states, we employed the screened hydrogenic approximation [26]. The ion abundance, level populations, and soft x-ray gain are calculated by postprocessing the temporal evolution of the T_e and n_e calculated by HYADES.

Figure 5 shows the calculated electron temperature T_e and density n_e of a tin plasma produced by the irradiation of two short laser pulses with a duration of 1.5 ps, separated by 1.2 ns. The intensities of the prepulse and main pulse are 1.6×10^{14} and 8×10^{14} W/cm^3, respectively. A pedestal level of 10^{12} W/cm^2 is assumed between two pulses to reproduce our present experimental conditions. The solid lines 1, 2, 3, and 4 are T_e and n_e at the peak of the main pulse, at 20 ps before the main pulse, at 40 ps after the main pulse, and at 100 ps after the main pulse, respectively, in the presence of the pedestal. In Fig. 5(b), traces 3 and 4 are almost the same as trace 1. This means that the electron density profile, which is determined by hydrodynamics motion, does not change substantially in 100 ps. The dashed lines are the T_e and n_e at 20 ps before the main pulse without the pedestal. It is found that the pedestal of the laser pulses sustains an electron temperature of the preplasma of nearly 200 eV during the expansion; otherwise it goes down below 50 eV before the arrival of the main pulse.

Figure 6 shows the tin soft x-ray gain and the average charge (z^*) of the plasma in the presence of the pedestal, where $z^* = 22$ means that the average ionic stage is the nickel-like ions. The time is measured from the peak of the main pulse. The gain is calculated by use of Eq. (2) under the condition $I_\nu = 0$, i.e., a Voigt profile is assumed for the laser line. The Doppler broadening and the collision and natural broadening are determined by the HYADES and WHIAM codes. Substantial gain is generated at around 40 ps with the pedestal effect. This calculated delay (40 ps) is longer compared with an experiment [27] and another theoretical model [28]. This is partly because the present case treats a high-*z* element ($z = 50$) compared with the above two references ($z = 47$ for Ref. [27] and 22 for Ref. [28]). Furthermore, in our calculation, the averaged charge of the ions just before the main pulse is ~15, and the ionization time to the nickel-like ion

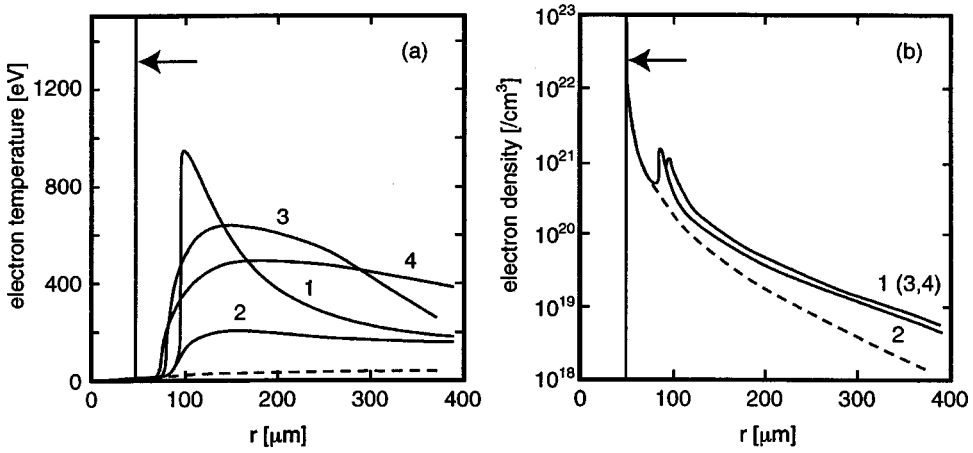

FIG. 5. The plasma parameters [electron temperature (a) and density (b)] of a plasma irradiated by two 1.5 ps laser pulses. The solid curves 1, 2, 3, and 4 are T_e and n_e at the peak of the main pulse (1), at 20 ps before the main pulse (2), at 40 ps after the main pulse (3), and at 100 ps after the main pulse (4), respectively, with pedestal level of 10^{12}W/cm^2. Dashed curve: T_e and n_e at the peak of the main pulse without pedestal level. The arrow shows the location of the initial target surface.

may induce this delay. It is noted that at around 40–100 ps after the main pulse, the calculated electron temperature and density of the gain region are ~500 eV and 5×10^{20} cm^{-3}, which are sufficient to generate substantial population inversion. The peak gain value is consistent with the experimental result. It is noted that if we assume only inhomogeneous broadening for the lasing line the peak gain becomes much higher than in the experiment.

In the case without the pedestal pulse, calculation shows that no substantial gain is generated. This is because fast recombination takes place substantially in the preformed plasma, and most of the energy of the main pulse is consumed before the ions in lower ionic states are reionized to nickel-like ions.

In Fig. 6(b), from a comparison of the solid line at +0 ps with the dashed line, it is obvious that the pedestal pulse plays a decisive role in retaining the nickel-like ion abundance in the plasma. This result together with the temporal profiles of T_e and n_e suggests that the present experimental condition is suitable for generating gains at these wavelengths, i.e., a pulse separation of ~1 ns can generate a long-scale-length plasma in the critical density region, and the pedestal level sustains the electron temperature until the arrival of the main pulse. It is noted that our calculation shows that below the pedestal level of 10^{11} W/cm^2 no substantial gain is generated; thus the lasing condition is sensitive to the pedestal level. In order to optimize the lasing condition, it is necessary to control the pedestal level, or use an additional long pulse with an irradiance of ~10^{12} W/cm^2 to control the ion abundance of the plasma. This is our objective in the near future.

IV. SUMMARY

We demonstrated gain saturation of nickel-like ion x-ray lasers at wavelengths of 13.9 and 12.0 nm using a compact CPA Nd:glass laser with an input energy of ~14 J. In this experiment, we employed quasitraveling-wave pumping using a six-step mirror, and the pumping energy to achieve gain saturation could be reduced to 2.5 J/mm. This result shows the possibility of a compact pumping system for x-ray lasers in the shorter-wavelength region. A theoretical calculation shows that the present experimental conditions are desirable for generating substantial gain.

ACKNOWLEDGMENTS

The authors are grateful to Dr. T. Arisawa of the Advanced Photon Research Center and Professor H. Takuma of the University of Electro-Communication for their help and useful comments. This work was supported in part by JAERI Foreign Researcher Invitation Program and Russian Fundation for Basic Research (RFBR) Grant No. 00-02-17060.

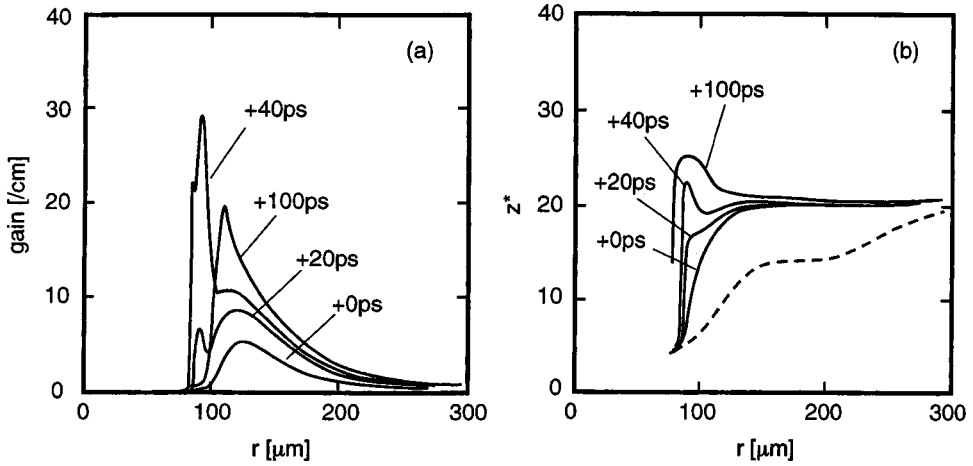

FIG. 6. Soft x-ray gain (a) and average charge (z^*) of the plasma (b) calculated using the temporal evolution of the density and temperature shown in Fig. 6. 0 ps corresponds to the peak of the main pulse. Dashed line shows z^* at 0 ps without the pedestal pulse.

[1] D. L. Matthews, P. L. Hagelstein, M. D. Rosen, M. J. Eckart, N. M. Ceglio, A. U. Hazi, H. Medecki, B. J. MacGowan, J. E. Trebes, B. L. Whitten, E. M. Campbell, C. W. Hatcher, A. M. Hawryluk, R. L. Kauffman, L. D. Pleasance, G. Rambach, J. H. Scofield, G. Stone, and T. A. Weave, Phys. Rev. Lett. **54**, 110 (1985).

[2] S. Suckewer, C. H. Skinner, H. Milchberg, C. Keane, and D. Voorhees, Phys. Rev. Lett. **55**, 1753 (1985).

[3] M. P. Kalachnikov, P. V. Nickles, M. Schnürer, W. Sandner, V. N. Shlyatsev, C. Danson, D. Neely, E. Wolfrum, J. Zhang, A. Behjat, A. Demir, G. J. Tallents, P. J. Warwick, and C. L. S. Lewis, Phys. Rev. A **57**, 4778 (1998).

[4] J. Dunn, A. L. Osterheld, R. Shepherd, W. E. White, V. N. Shlyaptsev, and R. E. Stewart, Phys. Rev. Lett. **80**, 2825 (1998).

[5] J. Dunn, A. L. Osterheld, J. Nilsen, J. R. Hunter, and V. N. Shlyaptsev, Phys. Rev. Lett. **84**, 4834 (2000).

[6] Y. Li, J. Dunn, J. Nilsen, T. W. Barbee, Jr., A. L. Osterheld, and V. N. Shlyaptsev, J. Opt. Soc. Am. B **17**, 1098 (2000).

[7] A. Klisnick, P. Zeitoun, D. Ros, A. Carillon, P. Fourcade, S. Hubert, G. Jamelot, C. L. S. Lewis, A. MacPhee, R. O'Rourcke, R. Keenan, P. Nickles, K. Janulewicz, M. Kalachnikov, J. Warwick, J. C. Chanteloup, A. Migus, E. Salmon, C. Sauteret, and J. P. Zou, J. Opt. Soc. Am. B **17**, 1093 (2000).

[8] J. Kuba, A. Klisnick, D. Ros, P. Fourcade, G. Jamelot, J. L. Miquel, N. Blanchot, and J. F. Wyart, Phys. Rev. A **62**, 043808 (2000).

[9] A. G. MacPhee, R. M. N. O'Rourke, C. L. S. Lewis, J. Y. Lin, A. Demir, G. J. Tallents, J. Collier, D. Neely, D. Ros, Ph. Zeitoun, S. P. McCabe, P. A. Simms, and G. J. Pert, in *Proceedings of X-Ray Lasers—1998*, edited by Y. Kato, H. Takuma, and H. Daido, IOP Conf. Proc. No. 159 (IOP, Kyoto, 1998), p. 75.

[10] J. C. Chanteloup, E. Salmon, C. Sauteret, A. Migus, Ph. Zeitoun, A. Klisnick, A. Carillon, S. Hubert, D. Ros, P. V. Nickles, and M. Kalachnikov, J. Opt. Soc. Am. B **17**, 151 (2000).

[11] J. L. Collier, C. N. Danson, R. M. Allott, H. M. R. Hutchinson, C. L. S. Lewis, D. Neely, D. A. Peplar, T. B. Winstone, and J. Zhang, in *Proceedings of X-Ray Lasers—1998* [9], p. 649.

[12] A. L. Osterheld, J. Dunn, and V. N. Shlyaptsev, in *Proceedings of X-Ray Lasers—1998* [9], p. 131.

[13] T. Fujimoto, J. Phys. Soc. Jpn. **54**, 2905 (1980).

[14] M. Kado, T. Kawachi, N. Hasegawa, M. Tanaka, K. Sukegawa, A. Nagashima, A. Sasaki, and Y. Kato, in *Proceedings of X-Ray Lasers—2000*, edited by G. Jamelot and A. Klisnick [J. Phys. IV **11,** 39 (2001)].

[15] T. Kawachi, M. Kado, M. Tanaka, N. Hasegawa, K. Sukegawa, K. Nagashima, F. Koike, A. Nagashima, and Y. Kato (unpublished).

[16] I. N. Ross, J. Boon, R. Corbett, A. R. Damerell, P. Gottfeldt, C. J. Hooper, M. H. Key, G. P. Kiehn, C. L. S. Lewis, and O. William, Appl. Opt. **26**, 1584 (1987).

[17] M. Koike, T. Namioka, E. Gullikson, Y. Harada, S. Ishikawa, T. Imazono, S. Mrowka, N. Miyata, M. Yanagihara, J. H. Underwood, K. Sano, N. Ogiwara, O. Yoda, and S. Nagai, Proc. SPIE **4146**, 163 (2000).

[18] G. J. Linford, E. P. Poressini, W. R. Sooy, and M. L. Spaeth, Appl. Opt. **13**, 379 (1974).

[19] M. Tanaka, T. Kawachi, M. Kado, N. Hasegawa, K. Sukegawa, A. Nagashima, and Y. Kato, in *Proceedings of the 13th International Conference on VUV Radiation Physics*, edited by M. Alterelli, Surface Rev. Lett. **9**, 641 (2002).

[20] W. T. Silfvast, *Laser Fundamentals* (Cambridge University Press, Cambridge, England, 1996).

[21] A. Yariv, *Quantum Electronics* (Wiley, New York, 1957).

[22] J. T. Larsen and S. M. Lane, J. Quant. Spectrosc. Radiat. Transf. **51**, 179 (1994).

[23] M. Klapisch and A. Bar-Shalom, J. Quant. Spectrosc. Radiat. Transf. **58**, 687 (1997).

[24] J. Zhang, A. G. MacPhee, J. Nilsen, J. Lin, W. Barbee, Jr., C. Danson, M. H. Key, C. L. S. Lewis, D. Neely, R. M. N. O'Rourke, G. J. Pert, R. Smith, G. J. Tallents, J. S. Wark, and E. Wolfrum, Phys. Rev. Lett. **78**, 3856 (1997).

[25] A. Sasaki, T. Utsumi, K. Moribayashi, M. Kado, M. Tanaka, N. Hasegawa, T. Kawachi, and H. Daido, J. Quant. Spectrosc. Radiat. Transf. **71**, 665 (2001).

[26] W. A. Lokke and W. H. Grasberger, Lawrence Livermore Laboratory Report No. UCRL-52276, 1977 (unpublished).

[27] A. Klisnick, J. Cuba, D. Ros, R. Smith, G. Jamelot, C. Chenais-Popovics, R. Keenan, S. J. Topping, C. L. S. Lewis, F. Strati, G. J. Tallents, D. Neely, R. Clarke, J. Collier, A. G. MacPhee, F. Bortolotto, P. V. Nickles, and K. A. Janulewicz, Phys. Rev. A **65**, 033810 (2002).

[28] J. Nilsen, Y. Li, and J. Dunn, J. Opt. Soc. Am. B **17**, 1084 (2000).